

A combined measurement of cosmic growth and expansion from clusters of galaxies, the CMB and galaxy clustering

David Rapetti^{1*}, Chris Blake², Steven W. Allen^{3,4}, Adam Mantz⁵, David Parkinson⁶ and Florian Beutler^{7,8}

¹ *Dark Cosmology Centre, Niels Bohr Institute, University of Copenhagen, Juliane Maries Vej 30, 2100 Copenhagen, Denmark*

² *Centre for Astrophysics & Supercomputing, Swinburne University of Technology, P.O. Box 218, Hawthorn, VIC 3122, Australia*

³ *Kavli Institute for Particle Astrophysics and Cosmology, Stanford University, 452 Lomita Mall, Stanford, CA 94305-4085, USA*

⁴ *SLAC National Accelerator Laboratory, 2575 Sand Hill Road, Menlo Park 94025, CA, USA*

⁵ *Kavli Institute for Cosmological Physics, University of Chicago, 5640 South Ellis Avenue, Chicago, IL 60637, USA*

⁶ *School of Mathematics and Physics, University of Queensland, Brisbane, QLD 4072, Australia*

⁷ *International Centre for Radio Astronomy Research, University of Western Australia, 35 Stirling Highway, Perth WA 6009, Australia*

⁸ *Lawrence Berkeley National Laboratory, 1 Cyclotron Road, Berkeley, CA 94720, USA*

Accepted 2013 March 21. Received 2013 March 21; in original form 2012 May 18

ABSTRACT

Combining galaxy cluster data from the *ROSAT* All-Sky Survey and the *Chandra* X-ray Observatory, cosmic microwave background data from the *Wilkinson Microwave Anisotropy Probe*, and galaxy clustering data from the WiggleZ Dark Energy Survey, the 6-degree Field Galaxy Survey and the Sloan Digital Sky Survey III, we test for consistency the cosmic growth of structure predicted by General Relativity (GR) and the cosmic expansion history predicted by the cosmological constant plus cold dark matter paradigm (Λ CDM). The combination of these three independent, well studied measurements of the evolution of the mean energy density and its fluctuations is able to break strong degeneracies between model parameters. We model the key properties of cosmic growth with the normalization of the matter power spectrum, σ_8 , and the cosmic growth index, γ , and those of cosmic expansion with the mean matter density, Ω_m , the Hubble constant, H_0 , and a kinematical parameter equivalent to that for the dark energy equation of state, w . For a spatially flat geometry, $w = -1$, and allowing for systematic uncertainties, we obtain $\sigma_8 = 0.785 \pm 0.019$ and $\gamma = 0.570^{+0.064}_{-0.063}$ (at the 68.3 per cent confidence level). Allowing both w and γ to vary we find $w = -0.950^{+0.069}_{-0.070}$ and $\gamma = 0.533 \pm 0.080$. To further tighten the constraints on the expansion parameters, we also include supernova, Cepheid variable and baryon acoustic oscillation data. For $w = -1$, we have $\gamma = 0.616 \pm 0.061$. For our most general model with a free w , we measure $\Omega_m = 0.278^{+0.012}_{-0.011}$, $H_0 = 70.0 \pm 1.3 \text{ km s}^{-1} \text{ Mpc}^{-1}$ and $w = -0.987^{+0.054}_{-0.053}$ for the expansion parameters, and $\sigma_8 = 0.789 \pm 0.019$ and $\gamma = 0.604 \pm 0.078$ for the growth parameters. These results are in excellent agreement with GR+ Λ CDM ($\gamma \simeq 0.55$; $w = -1$) and represent the tightest and most robust simultaneous constraint on cosmic growth and expansion to date.

Key words: cosmological parameters – cosmology: observations – X-ray: galaxies: clusters – cosmic microwave background – large-scale structure of Universe

1 INTRODUCTION

The unexpected measurement from type Ia supernova (SNIa) data of late-time cosmic acceleration by Riess et al. (1998) and Perlmutter et al. (1999) initiated a series of theoretical and observational efforts to unveil the na-

ture of its underlying cause. However, to this day it is still unclear whether the origin of this phenomenon is due to a new energy component, spurious cosmological assumptions, or modifications of gravity at large scales. A number of theoretical approaches and observational probes have been developed to investigate these different possibilities (for recent reviews see Copeland et al. 2006; Frieman et al. 2008; Allen et al. 2011; Clifton et al. 2012;

* Email: drapetti@dark-cosmology.dk

Weinberg et al. 2012). Current data on the energy content, geometry, and expansion and growth histories of the Universe do not show any deviation from the standard cosmological paradigm, Λ CDM (Allen et al. 2008; Mantz et al. 2008, 2010a; Vikhlinin et al. 2009; Percival et al. 2010; Reid et al. 2012; Conley et al. 2011; Blake et al. 2011a,b, 2012; Suzuki et al. 2012; Hinshaw et al. 2012). However, the cosmological constant model suffers from well-known, serious theoretical problems that present-day dark energy models have not been able to improve upon. For modified gravity models, various approaches have been developed¹: parameterized frameworks (Hu & Sawicki 2007; Bertschinger & Zukin 2008; Amin et al. 2008), consistency tests of GR (Linder 2005; Linder & Cahn 2007; Di Porto & Amendola 2008; Zhang et al. 2007; Nesseris & Perivolaropoulos 2008; Acquaviva et al. 2008), and alternative theories of gravity (Dvali et al. 2000; Carroll et al. 2004; Arkani-Hamed et al. 2004; Nicolis et al. 2009; de Rham et al. 2011). Recent works have used a variety of experiments and data sets to constrain gravity properties and models and found no significant deviations from GR (see e.g. Schmidt et al. 2009; Rapetti et al. 2009, 2010; Reyes et al. 2010; Daniel et al. 2010; Zhao et al. 2010, 2012; Giannantonio et al. 2010; Wojtak et al. 2011; Hojjati et al. 2011; Lombriser et al. 2012; Hudson & Turnbull 2012; Basilakos & Pouri 2012; Samushia et al. 2013; Simpson et al. 2013). To further test the overall standard paradigm, GR+ Λ CDM, it is crucial to use data sets able to robustly constrain the key properties of the model, and to combine complementary data sets to break the degeneracies between the model parameters.

Rapetti et al. (2010, hereafter R10) tested GR using *ROSAT* All-Sky Survey (RASS) and *Chandra* X-ray Observatory (CXO) data of cluster abundance and scaling relations (Mantz et al. 2010a,b, hereafter M10a,b). R10 obtained strong constraints on GR, even when marginalizing over conservative systematic and astrophysical modeling uncertainties in the evolution of the cluster X-ray luminosity-mass relation. When combining the cluster growth data with measurements of the anisotropies in the cosmic microwave background (CMB) from the *Wilkinson Microwave Anisotropy Probe* (*WMAP*; Spergel et al. 2003, 2007; Komatsu et al. 2009; Dunkley et al. 2009; Komatsu et al. 2011; Hinshaw et al. 2012; Bennett et al. 2012, and companion papers), they highlighted a large degeneracy between γ and σ_8 , which limited the constraints on each parameter individually. Here we include complementary data that break this degeneracy. In particular, we use measurements of the growth rate and the Hubble parameter from joint redshift space distortions (RSD) and Alcock-Paczynski (AP) effect constraints (Blake et al. 2011c, hereafter B11) from the WiggleZ Dark Energy Survey (WiggleZ; Drinkwater et al. 2010). We also use a low redshift RSD constraint (Beutler et al. 2012) from the final data release (DR3) of the 6-degree Field Galaxy Survey (6dFGS; Jones et al. 2009) and an RSD and AP constraint from the latest data release (DR9) of the Sloan Digital Sky Survey

(SDSS) III Baryon Oscillation Spectroscopic Survey (BOSS; Reid et al. 2012).

In addition to our primary data sets, and to tighten the constraints on the expansion parameters, we also present results including data from the Union II SNIa sample (Suzuki et al. 2012), baryon acoustic oscillation (BAO) measurements from a combined analysis (Percival et al. 2010) of 2-degree Field Galaxy Redshift Survey (2dFGRS; Colless et al. 2003) and SDSS-II DR7 (Abazajian et al. 2009) data as well as from a recent analysis (Reid et al. 2012) of SDSS-III BOSS data at a higher redshift, and H_0 measurements from the Supernovae and H_0 for the Equation of State program (SH0ES; Riess et al. 2011).

We find that by combining cluster, CMB and galaxy data we are able to break the key degeneracies between γ and σ_8 and obtain tight and robust constraints on cosmic expansion and growth. We model the expansion primarily with Ω_m , H_0 , and w and the growth with σ_8 and γ . We find that, individually, the CMB and galaxy data have large degeneracies in the growth plane but that, crucially, these degeneracies are nearly orthogonal. The individual and combined constraints from cluster, CMB and galaxy data are consistent with one another, making this a very robust measurement, and in good agreement with GR and Λ CDM. While individually clusters provide the tightest constraints in the growth plane, the combination of clusters, the CMB and galaxies provides significantly improved constraints and arguably the most robust measurement of cosmic structure growth to date.

2 COSMOLOGICAL MODEL

We adopt a purely phenomenological model to conveniently test the consistency of current observations with both the cosmic expansion history and the cosmic growth history predicted by Λ CDM+GR.

Our model assumes neither the existence of a new component, dark energy, nor a modification of GR. Instead, the parameters of the model represent departures from key kinematical and dynamical features of Λ CDM+GR. Deviations from such benchmarks would indicate disagreement of the observed evolution of the background and density perturbations with the standard cosmological paradigm.²

2.1 Cosmic expansion history

We model the expansion history using the evolution parameter $E(a) \equiv H(a)/H_0$, where $H(a)$ is the Hubble parameter as a function of the scale factor a and H_0 its present-day value. We parameterize $E(a)$ as follows

$$E(a) = \left[\Omega_m a^{-3} + (1 - \Omega_m) a^{-3(1+w)} \right]^{1/2}. \quad (1)$$

¹ Similar approaches can also be used to study clustering dark energy models.

² Note that different physical scenarios can cause similar departures from this paradigm. For example, specific models of clustering or interacting dark energy and of modified gravity might provide similar deviations from the density perturbations of Λ CDM+GR.

Ω_m is the present, mean matter density in units of the critical density of the Universe and w a kinematical parameter inspired by the dark energy equation of state. Since for our test we do not assume any particular scenario for cosmic acceleration, such as dark energy, we use w only to conveniently fit expansion history data, matching Λ CDM for $w = -1$. Below, we present results for two expansion models, $w = -1$ (Λ CDM) and w constant (w CDM). For both cases, we assume a spatially flat geometry (i.e., the curvature energy density $\Omega_k = 0$)³.

2.2 Cosmic growth and cluster abundance

We model the growth history at late times by parameterizing the linear growth rate of density perturbations on large scales, $f(a)$, as a power law of the evolving mean matter density, $\Omega_m(a) = \Omega_m a^{-3} E(a)^{-2}$, such as (Peebles 1980; Wang & Steinhardt 1998; Linder 2005)

$$f(a) \equiv \frac{d \ln \delta}{d \ln a} = \Omega_m(a)^\gamma, \quad (2)$$

where γ is the growth index⁴, for which we recover GR when $\gamma \simeq 0.55$.⁵ $\delta \equiv \delta \rho_m / \rho_m$ is the ratio of the comoving matter density fluctuations, $\delta \rho_m$, with respect to the cosmic mean, ρ_m . While at early times we assume GR, for $z < z_t$ we obtain $\delta(z)$ from equation 2 using as an initial condition $\delta(z_t)$ calculated within GR. Normalizing $\delta(z)$ to $\delta(z_t)$, we obtain the growth factor, $D(z) \equiv \delta(z)/\delta(z_t)$. Here we use $z_t = 30$, which is well within the dark matter dominated era, when $f(a) \sim 1$ for both the γ -model (equation 2) and GR. We then calculate the matter power spectrum of such fluctuations for a given wavenumber, k , as

$$P(k, z) \propto k^{n_s} T^2(k, z_t) D(z)^2, \quad (3)$$

where $T(k, z_t)$ is the matter transfer function of GR in the synchronous gauge at redshift z_t and n_s the primordial scalar spectral index.

The variance of the linearly evolved density field, smoothed by a spherical top-hat window function of comoving radius R enclosing mass $M = 4\pi \rho_m R^3/3$, is

$$\sigma^2(M, z) = \frac{1}{2\pi^2} \int_0^\infty k^2 P(k, z) |W_M(k)|^2 dk, \quad (4)$$

³ Using cluster, CMB and SNIa data, Rapetti et al. (2009) found a negligible correlation between Ω_k and γ . They also showed that the constraints on γ were not significantly weaker when including Ω_k as a free parameter. Note also that if Ω_k were included as a free parameter, an extension of equation 2 proposed by Gong et al. (2009) would fit better the predictions from GR.

⁴ Many models of modified gravity predict a growth index that varies with time and length scale, $\gamma(a, k)$. Note again, though, that here we do not use this parameter as a diagnostic of the true theory of gravity, but rather as a consistency test for GR.

⁵ For current results, this value is a good approximation to be used as a GR reference. At higher accuracy, though, the growth index of GR has relatively small redshift and background parameter dependencies (see e.g. Polarski & Gannouji 2008).

where $W_M(k)$ is the Fourier transform of the window function. From this expression, σ_8^2 is defined as the $z = 0$ variance in the density field at scales of $8h^{-1}$ Mpc, where σ_8 is widely used as a parameter for the normalization of the matter power spectrum.

Here we use $\sigma(M, z)$ to calculate the abundance of dark matter halos as a function of mass and redshift

$$n(M, z) = \int_0^M \mathcal{F}(\sigma, z) \frac{\rho_m}{M'} \frac{d \ln \sigma^{-1}}{d M'} dM', \quad (5)$$

where $\mathcal{F}(\sigma, z)$ is a convenient fitting formula obtained from large N-body simulations of dark matter particles (Tinker et al. 2008),

$$\mathcal{F}(\sigma, z) = A \left[\left(\frac{\sigma}{b} \right)^{-a} + 1 \right] e^{-c/\sigma^2}. \quad (6)$$

The parameters of this formula have a generic redshift dependence of the form $x(z) = x_0(1+z)^{\epsilon \alpha_x}$, with x representing A, a, b or c . The values for each x_0 and α_x are given in Tinker et al. (2008). As in M10a, we introduce an additional parameter, ϵ , to account for residual systematic uncertainties in the evolution of $\mathcal{F}(\sigma, z)$ due to non- Λ CDM scenarios. Remarkably, $\mathcal{F}(\sigma, z)$ encapsulates the non-linear cosmic growth history and appears to be almost universal for a wide range of cosmologies (see R10 for more details).

We marginalize over the uncertainties in the parameters of $\mathcal{F}(\sigma, z)$, accounting for their covariance and for additional systematic uncertainties due to e.g. the presence of baryons following the method described in M10a. Note, though, that as shown in M10a the uncertainties in $\mathcal{F}(\sigma, z)$ are subdominant in the analysis. R10 also verified that ϵ is essentially uncorrelated with γ .

2.3 Integrated Sachs-Wolfe effect

In our CMB analysis we include the constraint on γ from the Integrated Sachs-Wolfe (ISW) effect of the CMB using the method and assumptions described by Rapetti et al. (2009, 2010). In brief, the low multipoles of the CMB are sensitive to the growth of cosmic structure due to the effect of the time-varying gravitational potentials of large scale structures on the CMB photons crossing them. We calculate the contribution of these photons to the temperature anisotropy power spectrum as (Weller & Lewis 2003)

$$\Delta_l^{\text{ISW}}(k) = 2 \int dt e^{-\tau(t)} \phi'_{j_l} [k(t - t_0)], \quad (7)$$

where t is the conformal time and t_0 its present-day value, τ the optical depth to reionization, $j_l(x)$ the spherical Bessel function for the multipole l , and ϕ' the conformal time variation of the gravitational potential. Taking the derivative of the Poisson equation with respect to t , we calculate the latter quantity for the γ -model⁶ as $\phi' = 4\pi G a^2 k^{-2} \mathcal{H} \delta \rho_m [1 - \Omega_m(a)^\gamma]$, where \mathcal{H} is the conformal Hubble parameter. Since the ISW effect is only relevant for

⁶ Since here we are testing GR, we assume no contributions to ϕ from the anisotropic stress and energy flux of the Weyl tensor (Challinor & Lasenby 1999).

$z < 2$, as an initial condition to solve this equation we match $\Delta_l^{\text{ISW}}(k)$ to that of GR at $z_t = 2$.⁷

Note, however, that the constraining power on γ from the ISW effect is small compared to that of the cluster data (Rapetti et al. 2009). For the current analysis, the primary relevance of the CMB is its ability to tightly constrain the combination of growth parameters σ_8 and γ (see Section 5).

2.4 The Alcock-Paczynski effect and redshift-space distortions

The Alcock-Paczynski test is a geometrical means of probing the cosmological model by a comparison of the observed tangential and radial dimensions of objects which are assumed to be isotropic in the correct choice of model. It can be applied to the 2-point statistics of galaxy clustering if the redshift space distortions, the principal additional source of anisotropy, can be successfully modelled (Ballinger et al. 1996; Matsubara & Suto 1996; Matsubara 2000; Seo & Eisenstein 2003; Simpson & Peacock 2010). By equating radial and tangential physical scales, the AP test determines the observable $F(z) = (1+z)D_A(z)H(z)/c$, where $D_A(z)$ is the physical angular diameter distance and c is the speed of light.

In the model fit for $F(z)$, the normalized growth rate, $f\sigma_8(z)$, is determined simultaneously. Here $f(z)$ is again the logarithmic rate of change of the growth factor at redshift z (see equation 2) and $\sigma_8(z) = [D(z)/D(0)]\sigma_8$. In B11, RSD were modelled using the fitting formulae provided by Jennings et al. (2011) to determine the density-velocity and velocity-velocity power spectra, marginalizing over a linear bias factor. Tests were performed to ensure that the results were not very sensitive to the model used for the non-linear RSD, the real-space power spectrum, or the range of scales fitted ($k_{\text{max}} < 0.2 h \text{ Mpc}^{-1}$, for the measurements used here).

For a low-redshift survey such as 6dFGS, the Alcock-Paczynski distortion is negligible (since distances in $h^{-1} \text{ Mpc}$ are approximately independent of the assumed cosmological model)⁸. For 6dFGS, the growth rate measurement of Beutler et al. (2012) was obtained by again assuming the model of Jennings et al. (2011) to described non-linear RSD.

For the BOSS measurements of the RSD and AP effect, the modeling of the matter density and velocity fields was performed following the approach of Reid & White (2011). The latter uses perturbation theory to calculate the non-linear redshift space clustering of halos in the quasilinear regime and the halo model framework to describe the galaxy-halo relation. This model was tested against a large set of galaxy catalogs from N-body simulations and only fit over those scales where the quasilinear velocity field was thought to dominate the signal and the small-scale random velocities could be simply modeled and marginalized over.

For all the RSD and AP effect measurements employed

in the paper (see Section 4.2), the parameters used to fit the 2D galaxy power spectrum and galaxy correlation function data have negligible covariance with the parameters in the current analysis. Also, the linear model as well as the non-linear corrections assumed in those analyses lie within the GR+ Λ CDM paradigm tested here⁹.

3 PHYSICS OF THE OBSERVABLES

In this section, we describe the physical mechanisms behind the principle degeneracies between our most relevant growth and expansion parameters, for each of our primary observations.

3.1 CMB anisotropies

From the normalization and tilt of the CMB temperature anisotropy power spectrum, we can primarily constrain the scalar amplitude and spectral index of primordial fluctuations; from the position of its first peak, the mean energy density of curvature and dark energy; and from the amplitudes of the second and third peaks, those of dark and baryonic matter. These measurements provide strong constraints on the content of the background energy density and its linear density fluctuations at high redshift. For a given value of the growth index, γ , these translate into tight constraints on the amplitude of the matter power spectrum today, σ_8 . A model with faster perturbation growth, i.e. with a small γ , implies large fluctuations today, i.e. large σ_8 , and vice-versa. This provides a large, negative correlation between σ_8 and γ (see Figure 1). At low redshift, the ISW effect of the CMB data (see Section 2.3) constrains γ , which is otherwise unconstrained by this data set.

3.2 Distribution of galaxies

From measurements of the anisotropic clustering of galaxies, we use constraints on the product $f(z)\sigma_8(z)$ and on the quantity $F(z)$, where the latter are purely expansion history constraints, i.e. on $\Omega_m(z)$. Both of these constraints, from RSD and AP effect measurements respectively, are required to measure $\gamma = \ln f(z)/\ln \Omega_m(z)$ from galaxy data alone.¹⁰ The current uncertainty on the linear galaxy bias, $b(z)$, limits the ability to measure σ_8 from the normalization of the galaxy power spectrum, which scales with $\sigma_8(z)b(z)$, and to measure $f(z)$ using RSD constraints on $f(z)/b(z)$, as previously commonly used. As proposed by Song & Percival (2009), here we use instead RSD constraints on $f(z)\sigma_8(z)$, which are independent of $b(z)$, and obtain a positive correlation between γ and σ_8 (see Figure 1) for a Λ CDM expansion model and data within a relatively low- z range, where $f(z)$ increases towards 1. The faster the perturbations grow (small γ), the smaller the present-day perturbation amplitude, σ_8 , needs to be to provide the same amount

⁷ For our analysis, the difference from calculating $\delta(z)$ using z_t equals to 2 or 30 is negligible since both redshifts are well within the dark matter dominated era, when $f(a)$ tends to 1 for any γ .

⁸ Beutler et al. (2012) calculated the uncertainties in $F(z)$ and showed that they are unimportant.

⁹ The non-linear modeling from Jennings et al. (2011) used in the WiggleZ and 6dFGS analyses also encompasses a range of quintessence dark energy models.

¹⁰ In the same way as for the AP effect, the addition of the BAO constraints on $\Omega_m(z)$ improves significantly the measurement of γ for the combination gal+BAO (see the right panel of Figure 1).

of anisotropy in the distribution of galaxies at redshift z . At higher- z , where $f(z) \sim 1$ and $f(z)\sigma_8(z) \sim \sigma_8(z)$, the correlation between γ and σ_8 becomes negative (see Section 3.3). Adding high- z data from future missions will then help to break the large degeneracy of the current data between γ and σ_8 .

3.3 Cluster abundance and masses

For clusters, we have direct constraints on $\sigma_8(z)$ and $\Omega_m(z)$ from abundance, mass calibration and gas mass fraction data (see Sections 2.2 and 4.1). $\sigma_8(z)$ measurements provide us with constraints not only on $\sigma_8(z=0)$, from the local cluster mass function, but also on the growth rate $f(z) = -(1+z)d\ln\sigma_8(z)/dz$. Together, the constraints on $\sigma_8(z)$ and $\Omega_m(z)$ constrain γ .

The evolution of $\sigma_8(z) = \sigma_8 e^{-g(z)}$ depends on γ , Ω_m and w as follows

$$g(z) = \int_0^z (1+z')^{-1} [p(z') - 1]^{-\gamma} p(z')^\gamma dz' \quad (8)$$

$$= (3w\gamma)^{-1} [\lambda(z) - \lambda(0)], \quad (9)$$

where $\lambda(z) = [p(z) - 1]^{1-\gamma} p(z)^\gamma {}_2F_1[1, 1; 1 + \gamma; p(z)]$, ${}_2F_1$ is a hypergeometric function, $p(z) = p_0(1+z)^{-3w}$ and $p_0 = \Omega_m/(\Omega_m - 1)$. In practice, a negative degeneracy between σ_8 and γ exists due to the limited precision of cluster mass estimates, but it is notably smaller than those described above (see Figure 1). Within the precision of the data, indistinguishable cluster count evolution can be produced by models with e.g. σ_8 of 0.8 and a growth rate consistent with GR, or with a slightly larger present-day amplitude and faster growth (smaller γ), for which $\sigma_8(z)$ decreases with z a bit more steeply.

For the $\gamma+w$ CDM model, the dependence of $\sigma_8(z)$ on the product $w\gamma$ implies a negative correlation on the w, γ plane (see Figure 2). Within the precision of the data, a fast expansion history (small w) can be mimicked by a slow growth history (large γ), and vice-versa.

4 DATA ANALYSIS

4.1 Galaxy cluster data

For clusters we use two experiments: growth of structure (M10a,b) and gas mass fraction (f_{gas} ; Allen et al. 2008)¹¹.

Following the methods developed by M10a,b for the cluster growth analysis, we self-consistently and simultaneously combine X-ray survey and follow-up observations to obtain the best constraints possible while accounting fully for selection biases. We employ the survey data to determine cluster abundances and the follow-up data to calibrate cluster masses from three observables: luminosity, temperature and X-ray emitting gas mass. For the survey data we employ three wide-area cluster samples drawn from RASS: the Bright Cluster Sample in the northern sky (BCS; $z < 0.3$ and $F_X(0.1 - 2.4 \text{ keV}) > 4.4 \times 10^{-12} \text{ erg s}^{-1} \text{ cm}^{-2}$), the

ROSAT-ESO Flux Limited X-ray sample in the southern sky (REFLEX; $z < 0.3$ and $F_X > 3.0 \times 10^{-12} \text{ erg s}^{-1} \text{ cm}^{-2}$), and the Bright Massive Cluster Survey with ~ 55 per cent sky coverage (Bright MACS; $0.3 < z < 0.5$ and $F_X > 2 \times 10^{-12} \text{ erg s}^{-1} \text{ cm}^{-2}$). To keep systematic uncertainties to a minimum and maintain a trivial constant scaling between X-ray gas mass and total mass, for all three samples we impose a lower luminosity cut of $2.5 \times 10^{44} h_{70}^{-2} \text{ erg s}^{-1}$ (0.1 – 2.4 keV) leaving a total of 78 clusters from BCS; 126 clusters from REFLEX; and 34 clusters from Bright MACS. In total we use 238 clusters. For 94 of these clusters, we employ follow-up observations from CXO or pointed observations from ROSAT (M10b; distributed along the same redshift range of the survey data $0 < z < 0.5$) to constrain simultaneously the luminosity-mass (L – M) and temperature-mass (T – M) relations using the model from M10b (see a brief description in Section 4.1.1).

For the f_{gas} analysis, we use the methods and data set of Allen et al. (2008) for 42 massive, hot ($kT > 5 \text{ keV}$), dynamically relaxed, X-ray luminous galaxy clusters spanning the redshift range $0.05 < z < 1.1$.

4.1.1 Scaling relations model

We model the L – M scaling relation as (M10b)

$$\langle \ell(m) \rangle = \beta_0^{\ell m} + \beta_1^{\ell m} m + \beta_2^{\ell m} \log_{10}(1+z), \quad (10)$$

with a log-normal intrinsic scatter at a given mass of

$$\sigma_{\ell m}(z) = \sigma_{\ell m}(1 + \sigma'_{\ell m} z), \quad (11)$$

where $\ell \equiv \log_{10}[L_{500}E(z)^{-1}/10^{44} \text{ erg s}^{-1}]$ and $m \equiv \log_{10}[E(z)M_{500}/10^{15} M_\odot]$. The subscript 500 refers to quantities measured within radius r_{500} , at which the mean, enclosed density is 500 times the critical density of the Universe at redshift z . We model the T – M scaling relation $\langle t(m) \rangle$, where $t \equiv \log_{10}(kT_{500}/\text{keV})$, and its scatter $\sigma_{tm}(z)$ using the same equations 10 and 11 but with the parameters $\beta_0^{tm}, \beta_1^{tm}, \beta_2^{tm}, \sigma_{tm}$ and σ'_{tm} instead of those with index ℓ . When $\beta_2^{\ell m} = 0$ and $\beta_2^{tm} = 0$ we have “self-similar” evolution of the L – M and T – M relations respectively (Kaiser 1986; Bryan & Norman 1998)¹². $\sigma'_{\ell m} = 0$ and $\sigma'_{tm} = 0$ correspond to scaling relations with non-evolving scatter.

M10b showed that current data do not require departures from self-similar evolution and constant scatter. R10 demonstrated that γ correlates weakly with departures from self-similarity and constant scatter in the L – M relation and negligibly for those in the T – M relation. Here we therefore assume self-similar evolution and constant scatter for both relations ($\beta_2^{\ell m} = \sigma'_{\ell m} = \beta_2^{tm} = \sigma'_{tm} = 0$).

4.2 Galaxy clustering data

For WiggleZ, a series of growth and expansion analyses have recently been released, and here we build on one in particular: the joint analysis of the AP effect and growth of structure presented by B11, which contains four redshift bins of

¹¹ Note that the cluster growth analysis employs the f_{gas} analysis to calibrate the masses for the scaling relations of Section 4.1.1 using gas mass as a proxy for total mass (see details in M10a).

¹² Self-similar evolution is entirely determined by the $E(z)$ factors in the definitions of ℓ , t and m .

width $\Delta z = 0.2$, spanning the redshift range $0.1 < z < 0.9$. The WiggleZ survey at the Australian Astronomical Observatory was designed to extend the study of large-scale structure over large cosmic volumes to higher redshifts $z > 0.5$, complementing SDSS observations at lower redshifts. The survey, which began in August 2006, completed observations in January 2011 and has obtained of order 200,000 redshifts for UV-bright emission-line galaxies covering of order 1000 square degrees of equatorial sky.

For the WiggleZ analysis we fit our cosmological models to the joint measurements of RSD and AP distortion presented by B11. For this, we use the constraints obtained by B11 as a bivariate Gaussian likelihood for $f\sigma_8(z)$ and $F(z)$, including the large correlations between them. From B11, we have four bins with effective redshifts $z = (0.22, 0.41, 0.60, 0.78)$ and $f\sigma_8(z) = (0.53 \pm 0.14, 0.40 \pm 0.13, 0.37 \pm 0.08, 0.49 \pm 0.12)$, $F(z) = (0.28 \pm 0.04, 0.44 \pm 0.07, 0.68 \pm 0.06, 0.97 \pm 0.12)$ and correlation coefficients $r = (0.83, 0.94, 0.89, 0.84)$.

For the 6dFGS analysis we use the growth rate of structure measurement obtained by Beutler et al. (2012). The 6dFGS is a combined redshift and peculiar velocity survey covering nearly the entire southern sky with the exception of a 10 degree band along the Galactic plane. Observed galaxies were selected from the 2MASS Extended Source Catalog (Jarrett et al. 2000) and the redshifts were obtained with the 6-degree Field multi-fibre instrument at the U.K. Schmidt Telescope between 2001 and 2006. The final 6dFGS sample contains about 125,000 galaxies in 5 bands distributed over $\sim 17,000$ square degrees with a mean redshift of $z = 0.052$.

For the analysis of the RSD from 6dFGS data we use the constraints obtained by Beutler et al. (2012) as a Gaussian likelihood for $f\sigma_8(z) = 0.423 \pm 0.055$ at an effective redshift $z = 0.067$.

The analysis of the SDSS-III BOSS results from Reid et al. (2012) are based on the high- z sample CMASS, which consists of 264,283 galaxies in the redshift range $0.43 < z < 0.7$ over 3,275 square degrees. As part of SDSS-III (Eisenstein et al. 2011), BOSS has imaged the South Galactic sky for an additional 3100 square degrees over SDSS-II. This has increased the total sky coverage of SDSS imaging to 14,055 square degrees. As its primary goal, BOSS targets for spectroscopy luminous galaxies selected from the SDSS imaging. Within BOSS, CMASS is a roughly volume-limited sample of massive, luminous galaxies (for more detail see e.g. Masters et al. 2011) tracing a cosmological volume at a high enough density to enable powerful statistical studies of large-scale structure.

For the analysis of the growth rate and AP effect measurements of CMASS BOSS, we use a bivariate Gaussian likelihood for $f\sigma_8(z) = 0.43 \pm 0.07$ and $F(z) = 0.68 \pm 0.04$ with a correlation coefficient $r = 0.87$ at an effective redshift $z = 0.57$ (Reid et al. 2012)¹³. Note that this redshift is similar to that of the third redshift bin of the WiggleZ analysis, $z = 0.6$. Due to the small overlap and the uncorrelated shot noise between the two surveys, their covariance should be

minimal. Importantly, the results obtained by the two independent experiments, which target very different galaxy types, and require very specific studies of their nonlinear properties and modeling uncertainties, are consistent.

4.3 CMB data

For the CMB analysis, we use the data and likelihood code¹⁴ from *WMAP*¹⁵. For the analyses including CMB data, we also fit for the mean physical baryon and dark matter densities, $\Omega_b h^2$ and $\Omega_c h^2$, the optical depth to reionization, τ , the logarithm of the adiabatic scalar amplitude, $\ln(A_s)$, which is related to σ_8 , and the adiabatic scalar spectral index, n_s . For these analyses, instead of H_0 we fit θ , the (approximate) ratio of the sound horizon at last scattering to the angular diameter distance, which is less correlated with other parameters than H_0 (Kosowsky et al. 2002). We also marginalize over the amplitude of the Sunyaev-Zel'dovich effect from galaxy clusters, $0 < A_{SZ} < 2$ (Spergel et al. 2007).

4.4 Additional data sets

We also present results including constraints from the Union II SNIa data set of Suzuki et al. (2012), the SH0ES program of Riess et al. (2011), and the BAO analyses of Percival et al. (2010), at two intermediate redshifts, and Reid et al. (2012), at a higher redshift.

The SNIa data set consists of a compilation of 580 SNIa from a variety of sources. For the likelihood analysis of these data we use the COSMOMC module¹⁶ of Suzuki et al. (2012), including their treatment of the systematic errors.

For the BAO analysis, we use the results and methods of Percival et al. (2010), based on 2dFGRS (Colless et al. 2003) and SDSS-II DR7 (Abazajian et al. 2009) data, by including bivariate Gaussian constraints on the ratio $d_z \equiv r_s(z_d)/D_v(z)$ at $z = 0.2$ and $z = 0.35$, with the corresponding covariance between $d_{0.2}$ and $d_{0.35}$, where $r_s(z_d)$ is the sound horizon at the drag epoch¹⁷ and $D_v(z) \equiv$

¹⁴ <http://lambda.gsfc.nasa.gov/>

¹⁵ Here we use the five-year *WMAP* data (Dunkley et al. 2009; Komatsu et al. 2009, and companion papers). For various of our results we have incorporated the galaxy data by importance sampling MCMC chains that had clusters and *WMAP*5 data. Note that, for Λ CDM and w CDM models, the constraints on $\Omega_m h^2$, $\Omega_c h^2$ (see comments on this parameter in Section 5.2), w , H_0 and σ_8 from *WMAP*7 data alone do not differ significantly from those of *WMAP*5 (a maximum of 15 per cent in the errors of these parameters and much less in most cases), and even less when combined with additional data sets as those in Section 4.4. We therefore expect a relatively small impact on the results from using *WMAP*7 instead. The new *WMAP*9 data, which appeared in the last stage of the present work, have up to 36 per cent better errors than *WMAP*5 for those parameters, and promises then a somewhat larger impact on the results.

¹⁶ <http://supernova.lbl.gov/Union/>

¹⁷ To calculate z_d we use the exact expression (see e.g. appendix B of Hamann et al. 2010) instead of the approximate fitting formula of Eisenstein & Hu (1998). Note, however, that since Percival et al. (2010) and Reid et al. (2012) used the latter formula to fit the data, our results of the sound horizon need to be appropriately rescaled (see again Hamann et al. 2010). Besides being more accurate, the exact calculation of z_d is independent

¹³ For the results in Section 5 that include these and the distance-scale constraints from the BAO signature in the CMASS BOSS data, we extend this likelihood to account for the correlations between these three measurements as discussed in Section 4.4.

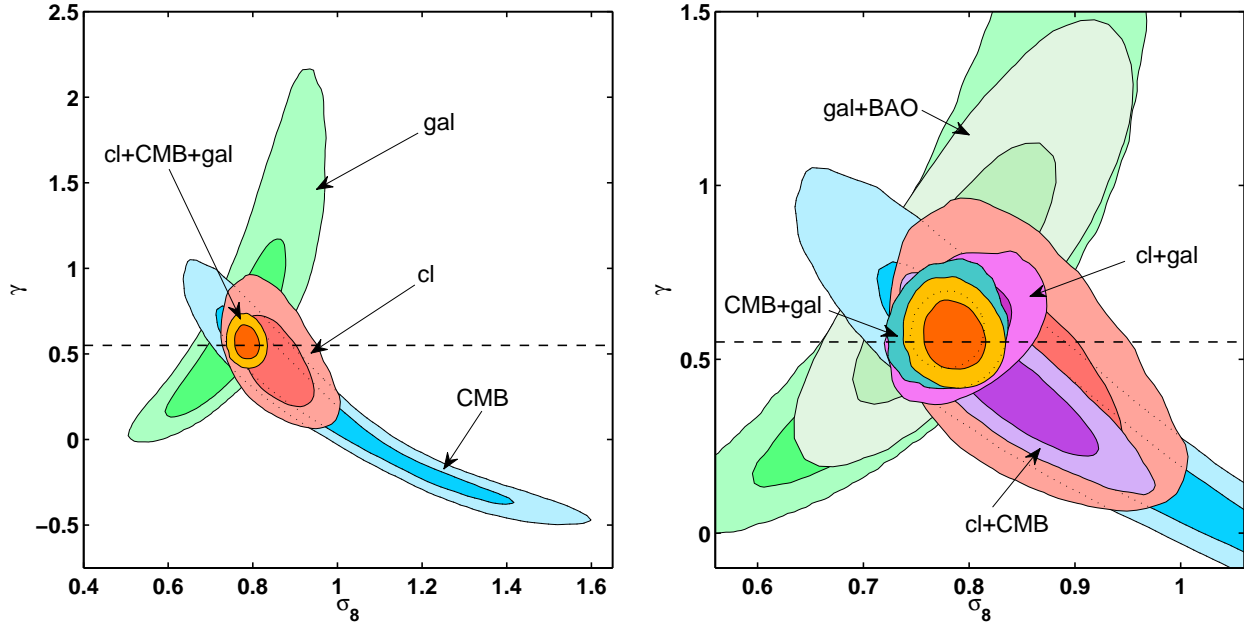


Figure 1. 68.3 and 95.4 per cent confidence contours in the σ_8, γ plane for the $\gamma + \Lambda$ CDM model. In the left panel, results are shown for the following individual data sets: galaxy growth (gal; green contours), CMB (blue contours) and cluster growth (cl; red contours). In the right panel, the same results are shown (for comparison purposes) together with the following combinations: cl+CMB (purple contours), cl+gal (magenta contours) and CMB+gal (turquoise contours). The combination of the three data sets breaks the degeneracies between γ and σ_8 and provides tight constraints on this plane (inner, gold contours). In the right panel, results are also shown for the combination gal+BAO (pale green contours). The horizontal, dashed lines mark $\gamma = 0.55$ (GR).

$[(1+z)^2 D_A(z)^2 c z / H(z)]^{1/3}$. Percival et al. (2010) showed that these results can also be recast as approximately independent Gaussian constraints on $d_{0.275}$ and the ratio of the distance scales $D_v(0.35)/D_v(0.2)$. For the BAO results of Reid et al. (2012), based on CMASS BOSS data, we extend the bivariate Gaussian likelihood of Section 4.2 to a trivariate Gaussian likelihood by including a constraint on $\alpha \equiv [d_z]_{\text{fiducial}}/d_z = 1.023 \pm 0.019$, at $z = 0.57$, and the corresponding correlation coefficients $r_{f\sigma_8\alpha} = -0.0086$ and $r_{F\alpha} = -0.080$ (see Section 6.4 of Reid et al. 2012).

Note that the overlap between the ranges in redshift of the SDSS-II DR7 luminous red galaxy sample ($0.16 < z < 0.47$) used in the Percival et al. (2010) results and the SDSS-III DR9 CMASS sample ($0.43 < z < 0.7$) used in the BOSS results (Reid et al. 2012) is very small (see this comparison e.g. in Anderson et al. 2012). Therefore, we assume that the two BAO measurements are essentially independent and can be straightforwardly combined.

For the SH0ES analysis, we use a Gaussian prior on $H_0 = 73.8 \pm 2.4 \text{ km s}^{-1} \text{ Mpc}^{-1}$. This measurement is based on *Hubble Space Telescope* optical and infrared data for over 600 Cepheid variables in the host galaxies of 8 nearby SNIa (Riess et al. 2011).

of the standard assumptions used to obtain the fitting formula, and therefore valid for other models. Interestingly, though, for the extended models used here we find no significant differences in the results obtained from using either calculation.

4.5 MCMC implementation

To calculate the parameter posterior probability distribution functions (pdf's) we use the Metropolis-Hastings Markov Chain Monte Carlo (MCMC) algorithm, as implemented in the code COSMOMC¹⁸ (Lewis & Bridle 2002). We employ a modified version of this code that includes additional modules for the likelihood analyses of the cluster growth experiment (M10a) and the f_{gas} experiment (Rapetti et al. 2005; Allen et al. 2008)¹⁹. In this version of the code, we have also incorporated the RSD, AP effect and BAO (BOSS) analyses as COSMOMC modules²⁰. We also use a modified version of the code CAMB²¹ (Lewis et al. 2000) that includes γ in the analysis of the ISW effect of the CMB data (Rapetti et al. 2009).

For our most general model, we simultaneously fit a total of 34 parameters. From these, 8 are cosmological parameters and 26 are used to model astrophysical variables and marginalize over systematic uncertainties: 1 for CMB (see Section 4.3), 7 for f_{gas} (see details in Allen et al. 2008) and 18 for cluster growth data (see Sections 2.2, 4.1.1, and M10a,b for full details).

¹⁸ <http://cosmologist.info/cosmomc/>

¹⁹ http://www.slac.stanford.edu/~drapetti/fgas_module/

²⁰ We use these and standard modules for the other data sets in Section 4.4 either to run new MCMC chains or to perform importance sampling on existing ones. For selected examples, we have explicitly checked that both methods provide the same results.

²¹ <http://camb.info/>

Table 1. Marginalized mean values and 68.3 per cent confidence limits for the γ + Λ CDM and γ + w CDM models using various subsets of the data. When the CMB data is not included the BBNS and SH0ES priors are used. For gal+BAO and γ + Λ CDM, a slightly tighter constraint than the prior on H_0 is obtained.

Data	Ω_m	H_0 (km s ⁻¹ Mpc ⁻¹)	w	σ_8	γ
cl	0.216 ^{+0.032} _{-0.032}	73.7 ^{+2.4} _{-2.4}	-1	0.856 ^{+0.054} _{-0.055}	0.469 ^{+0.175} _{-0.177}
cl+CMB	0.249 ^{+0.021} _{-0.021}	72.5 ^{+2.1} _{-2.1}	-1	0.844 ^{+0.049} _{-0.049}	0.415 ^{+0.128} _{-0.126}
cl+gal	0.236 ^{+0.033} _{-0.034}	73.1 ^{+2.4} _{-2.4}	-1	0.795 ^{+0.030} _{-0.030}	0.586 ^{+0.090} _{-0.089}
gal+BAO	0.366 ^{+0.049} _{-0.049}	72.8 ^{+2.3} _{-2.3}	-1	0.795 ^{+0.063} _{-0.063}	0.780 ^{+0.255} _{-0.256}
CMB+gal	0.256 ^{+0.027} _{-0.027}	71.9 ^{+2.4} _{-2.4}	-1	0.779 ^{+0.023} _{-0.023}	0.588 ^{+0.073} _{-0.073}
cl+CMB+gal	0.254 ^{+0.022} _{-0.022}	72.2 ^{+2.0} _{-2.1}	-1	0.785 ^{+0.019} _{-0.019}	0.570 ^{+0.064} _{-0.063}
cl+CMB+gal+BAO	0.284 ^{+0.013} _{-0.013}	69.4 ^{+1.1} _{-1.1}	-1	0.789 ^{+0.019} _{-0.019}	0.618 ^{+0.063} _{-0.063}
cl+CMB+gal+SH0ES	0.247 ^{+0.017} _{-0.017}	72.8 ^{+1.5} _{-1.6}	-1	0.784 ^{+0.019} _{-0.019}	0.561 ^{+0.061} _{-0.061}
cl+CMB+gal+SNIa	0.264 ^{+0.019} _{-0.020}	71.3 ^{+1.8} _{-1.8}	-1	0.788 ^{+0.019} _{-0.019}	0.585 ^{+0.065} _{-0.064}
cl+CMB+gal+SNIa+BAO	0.284 ^{+0.012} _{-0.012}	69.4 ^{+1.1} _{-1.1}	-1	0.790 ^{+0.019} _{-0.019}	0.618 ^{+0.062} _{-0.062}
cl+CMB+gal+SNIa+SH0ES	0.255 ^{+0.015} _{-0.016}	72.1 ^{+1.5} _{-1.4}	-1	0.786 ^{+0.019} _{-0.019}	0.575 ^{+0.060} _{-0.060}
cl+CMB+gal+SNIa+SH0ES+BAO	0.277 ^{+0.011} _{-0.011}	70.2 ^{+1.0} _{-1.0}	-1	0.791 ^{+0.019} _{-0.019}	0.616 ^{+0.061} _{-0.061}
cl	0.220 ^{+0.034} _{-0.034}	73.7 ^{+2.4} _{-2.4}	-1.021 ^{+0.190} _{-0.187}	0.855 ^{+0.056} _{-0.057}	0.507 ^{+0.236} _{-0.242}
cl+CMB	0.240 ^{+0.030} _{-0.030}	74.4 ^{+4.4} _{-4.4}	-1.062 ^{+0.122} _{-0.122}	0.851 ^{+0.052} _{-0.052}	0.454 ^{+0.148} _{-0.149}
cl+gal	0.216 ^{+0.036} _{-0.035}	73.5 ^{+2.4} _{-2.4}	-0.865 ^{+0.109} _{-0.107}	0.812 ^{+0.035} _{-0.035}	0.502 ^{+0.102} _{-0.103}
gal+BAO	0.323 ^{+0.060} _{-0.060}	73.9 ^{+2.4} _{-2.4}	-1.199 ^{+0.176} _{-0.179}	0.721 ^{+0.081} _{-0.085}	0.616 ^{+0.265} _{-0.266}
CMB+gal	0.278 ^{+0.034} _{-0.034}	69.0 ^{+3.4} _{-3.4}	-0.909 ^{+0.081} _{-0.082}	0.772 ^{+0.023} _{-0.023}	0.526 ^{+0.088} _{-0.088}
cl+CMB+gal	0.263 ^{+0.024} _{-0.025}	70.6 ^{+2.7} _{-2.7}	-0.950 ^{+0.069} _{-0.070}	0.780 ^{+0.020} _{-0.020}	0.533 ^{+0.080} _{-0.080}
cl+CMB+gal+BAO	0.289 ^{+0.015} _{-0.015}	68.3 ^{+1.8} _{-1.8}	-0.941 ^{+0.073} _{-0.073}	0.783 ^{+0.020} _{-0.020}	0.562 ^{+0.086} _{-0.087}
cl+CMB+gal+SH0ES	0.248 ^{+0.017} _{-0.017}	72.4 ^{+1.8} _{-1.9}	-0.983 ^{+0.060} _{-0.059}	0.783 ^{+0.020} _{-0.020}	0.549 ^{+0.080} _{-0.080}
cl+CMB+gal+SNIa	0.267 ^{+0.019} _{-0.019}	70.1 ^{+1.9} _{-1.9}	-0.939 ^{+0.053} _{-0.053}	0.780 ^{+0.020} _{-0.020}	0.530 ^{+0.077} _{-0.076}
cl+CMB+gal+SNIa+BAO	0.288 ^{+0.013} _{-0.013}	68.6 ^{+1.4} _{-1.4}	-0.950 ^{+0.055} _{-0.056}	0.784 ^{+0.019} _{-0.019}	0.569 ^{+0.079} _{-0.079}
cl+CMB+gal+SNIa+SH0ES	0.255 ^{+0.015} _{-0.015}	71.6 ^{+1.5} _{-1.5}	-0.961 ^{+0.050} _{-0.051}	0.782 ^{+0.020} _{-0.020}	0.537 ^{+0.077} _{-0.076}
cl+CMB+gal+SNIa+SH0ES+BAO	0.278 ^{+0.012} _{-0.011}	70.0 ^{+1.3} _{-1.3}	-0.987 ^{+0.054} _{-0.053}	0.789 ^{+0.019} _{-0.019}	0.604 ^{+0.078} _{-0.078}

For analyses without CMB data, we fix n_s to 0.95 since, for such analyses, n_s is degenerate with σ_8 (see M10a). For these analyses, we also use Gaussian priors on H_0 from the SH0ES program (Riess et al. 2011), and $\Omega_b h^2 = 0.0213 \pm 0.0010$ from Big Bang Nucleosynthesis (BBNS) studies (Pettini et al. 2008).

5 RESULTS

5.1 Constraints on the γ + Λ CDM model

The left panel of Figure 1 shows the joint constraints in the σ_8, γ plane for the γ + Λ CDM model. The green contours show the constraints obtained from the RSD and AP effect data from WiggleZ, 6dFGS and CMASS BOSS (hereafter referred as galaxy/gal data); the blue contours those from the CMB data; and the red contours those from the cluster abundance and f_{gas} data (hereafter referred as cluster/cl data). Combining the cluster+CMB+galaxy data we obtain the tight constraints shown by the gold contours.

As shown in the figure, individually, the CMB and

galaxy data exhibit significant degeneracies in the σ_8, γ plane, as expected (see Section 3). For the cluster data, the correlation between these two parameters is much weaker, enabling independent constraints on both parameters.²² Importantly, the constraints from the three independent experiments (which are affected by very different systematic uncertainties) are in excellent agreement. This agreement motivates us to combine the constraints, leading to the results shown in the inner, gold contours. Combining the three data sets we obtain marginalized constraints on $\gamma = 0.570^{+0.064}_{-0.063}$ (in good agreement with GR) and $\sigma_8 = 0.785 \pm 0.019$ (see also Table 1).²³

²² When combining gal+BAO we also obtain results that are more comparable to those of the clusters due to the degeneracies broken by this combination (see further details in the text).

²³ For this paper, we quote marginalized mean values and central credible intervals. For the latter, equal fractions of the volume of the posterior lie on each side of the interval (see e.g. Hamann et al. 2007). Instead, in R10 results were presented using marginalized peak values and minimal credible intervals, for

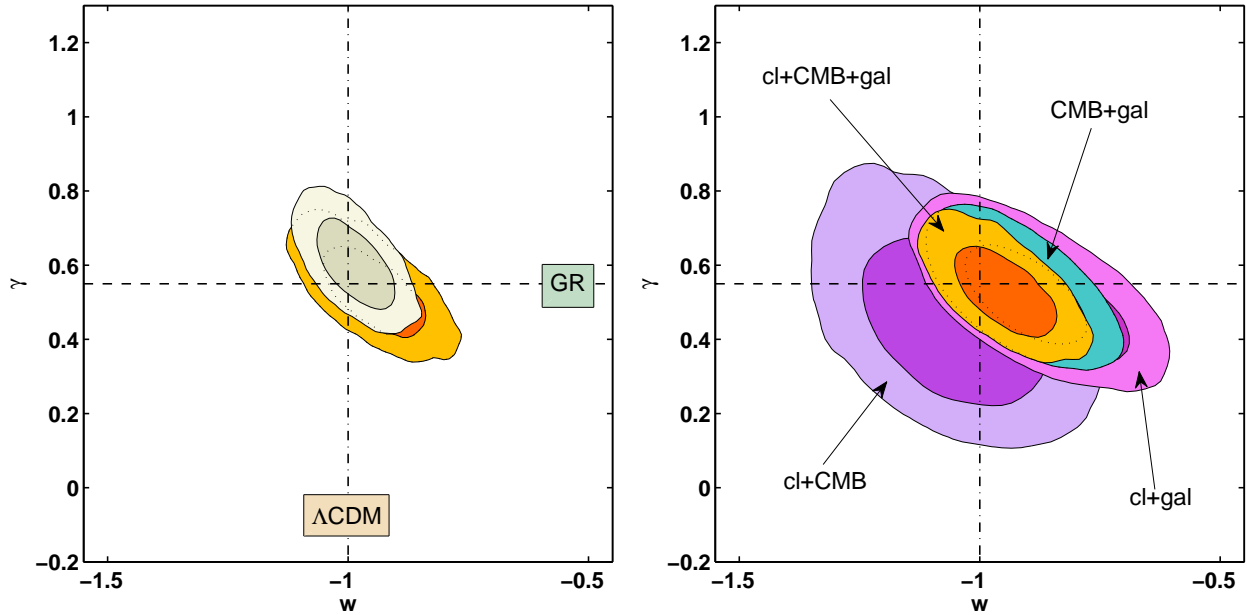


Figure 2. 68.3 and 95.4 per cent confidence contours in the w, γ plane for the $\gamma+w$ CDM model from cl+CMB+gal (gold contours in both panels) and the following combinations of data (right panel): cl+CMB (purple contours), cl+gal (magenta contours), and CMB+gal (turquoise contours). The platinum contours in the left panel correspond to adding SNIa+SH0ES+BAO to the combination of cl+CMB+gal. The horizontal, dashed lines mark $\gamma = 0.55$, the growth history for GR. The vertical, dot-dashed lines mark $w = -1$, the expansion history for Λ CDM. This figure shows that the results are simultaneously consistent with GR and Λ CDM.

If we also include SNIa, BAO and the SH0ES measurement of H_0 , the constraints on the growth parameters are, as expected, almost the same (see Table 1) although interestingly we obtain a small 4 per cent improvement in the error in γ . For this combination we also obtain improved, tight constraints on the expansion parameters $\Omega_m = 0.277 \pm 0.011$ and $H_0 = 70.2 \pm 1.0 \text{ km s}^{-1} \text{ Mpc}^{-1}$. It is worth noting that the addition of the BAO data alone provides almost the same improved constraints on the Ω_m, H_0 plane as those from adding all three data sets (see Table 1).

The right panel of Figure 1 shows a zoom into the central regions of the constraints shown in the left panel, together with the constraints for the combinations of cl+CMB data (purple contours), cl+gal data (magenta contours) and CMB+gal data (turquoise contours). The gold, tightest contours correspond again to the combination of the three data sets, cl+CMB+gal. Notably, the nearly orthogonal degeneracies of the CMB (blue contours) and galaxy (green contours) constraints allow their combination (turquoise contours) to provide tight marginalized constraints in the growth plane. The area enclosed by the 95.4 per cent confidence contour in the σ_8, γ plane is only slightly more than one third larger for CMB+gal than for the three data sets combined.

which the size of the interval is minimized. For approximately symmetric posteriors, such as those for our combined data, both choices provide similar results, although by construction those from the former tend to be slightly more conservative. For our individual data sets, for which the posteriors are less symmetric, we show full marginalized distributions in Figures 4 and 5.

As found by R10²⁴, for the cl+CMB data (purple contours) σ_8 and γ are highly correlated, with a correlation coefficient $\rho = -0.85$. The addition of the galaxy data breaks this degeneracy. With respect to constraints obtained from cl+CMB, those for the cl+CMB+gal provide more than a factor 2 reduction in the area enclosed by the 95.4 per cent confidence contour in the σ_8, γ plane.

In the right panel of the figure, we also show the constraints from the combination gal+BAO (pale green contours), for which both data sets come from the analysis of different properties of galaxy redshift surveys. Interestingly, even though the baryon acoustic oscillation data on their own provide only constraints on expansion parameters, those on Ω_m help in reducing the large degeneracies that the galaxy growth data has in the Ω_m, γ and Ω_m, σ_8 planes, with correlation coefficients of $\rho = 0.83$ and $\rho = 0.74$ for each plane. Adding BAO to gal we obtain then a significant improvement in the constraints on the growth plane σ_8, γ .

5.2 Constraints on the $\gamma+w$ CDM model

The left panel of Figure 2 shows the joint constraints in the w, γ plane for the $\gamma+w$ CDM model. For the combination of our primary data sets, cl+CMB+gal, we obtain the gold contours. For these, we find marginalized constraints on $w = -0.950^{+0.069}_{-0.070}$ and $\gamma = 0.533 \pm 0.080$ at the 68.3 per

²⁴ Note that the results presented in R10 were for a combination of cluster+CMB+SNIa+BAO data. However, the constraints on the σ_8, γ plane were primarily driven by the cluster+CMB data.

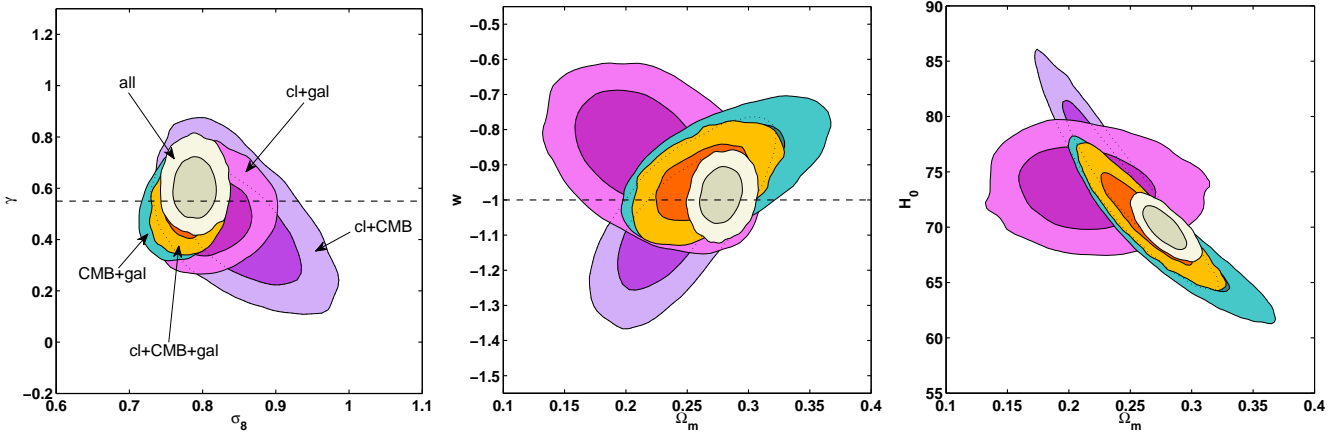


Figure 3. 68.3 and 95.4 per cent confidence contours in the growth plane σ_8, γ (left panel) and the expansion planes Ω_m, w (middle panel) and Ω_m, H_0 (right panel) for the $\gamma + w$ CDM model. The three panels show constraints from the following combinations of data sets: cl+CMB (purple contours), cl+gal (magenta contours), CMB+gal (turquoise contours), and cl+CMB+gal (gold contours). The platinum contours correspond to adding SNIa+SH0ES+BAO to the latter combination of data. The horizontal, dashed lines mark $\gamma = 0.55$ (GR; left panel) and $w = -1$ (Λ CDM; middle panel).

cent confidence level. These results are simultaneously consistent with GR and Λ CDM. The platinum contours in this panel show the joint constraints on the w, γ plane when we add SNIa+SH0ES+BAO to the cl+CMB+gal data²⁵. In this case, we find marginalized constraints of $w = -0.987^{+0.054}_{-0.053}$ and $\gamma = 0.604 \pm 0.078$. Again the results are consistent with GR+ Λ CDM.

In the right panel of the figure, the purple contours correspond to cl+CMB, the magenta contours to cl+gal, the turquoise contours to CMB+gal and the gold contours again to the combination of the three data sets. The horizontal, dashed and vertical, dot-dashed lines mark $\gamma = 0.55$ (GR) and $w = -1$ (Λ CDM), respectively.

Comparing the cl+CMB with the cl+CMB+gal results, we find 46 and 62 per cent improvements in the constraints on γ and σ_8 . It is also worth noting that the improvement in the joint measurement of w and γ is larger than that for each individual parameter. We find more than a factor 3 reduction in the area enclosed by the 95.4 per cent confidence contour of the joint w, γ constraints. Note that the correlation between w and γ increases from $\rho = -0.47$, for cl+CMB, to $\rho = -0.66$, for cl+CMB+gal, which suggests that additional constraints on w might also help improving those on γ . In fact, even though SNIa and SH0ES data provide direct additional constraints on only cosmic expansion parameters, for which we obtain e.g. a 27 per cent improvement on w when adding them to cl+CMB+gal, the combined, marginalized constraints on γ represent a small improvement of 4 per cent due to the correlation between w and γ . For these data sets combined, cl+CMB+gal+SNIa+SH0ES, the correlation in the w, γ plane is still of $\rho = -0.65$. Interestingly, the correlation between γ and $\Omega_c h^2$ is also relatively large, $\rho = 0.72$,²⁶

²⁵ From Table 1, note that the main additional constraint on this plane comes from the SNIa data. The SH0ES and BAO data, though, significantly help in constraining the combination of parameters Ω_m and H_0 .

²⁶ The correlation between γ and the CMB shift parameter,

which indicates that e.g. the significant improvements in the constraints on this parameter from the CMB measurements of the *Planck* satellite²⁷ should help with constraining γ .

Figure 3 shows constraints for the same model and subsets of the data for three different planes: the growth plane σ_8, γ (left panel) and the expansion planes Ω_m, w (middle panel) and Ω_m, H_0 (right panel). The left panel of this figure shows that the correlation between σ_8 and γ reduces dramatically from cl+CMB (purple contours), $\rho = -0.56$, to cl+CMB+gal (gold contours), a negligible $\rho = 0.08$. The reduction in the area enclosed by the 95.4 per cent confidence contour in this growth plane when adding gal to the cl+CMB data is substantial.

The platinum contours in the three panels correspond to the constraints obtained when adding SNIa+SH0ES+BAO to the cl+CMB+gal data. The improvement in the growth plane of the left panel of the figure is small while those in the expansion planes of the middle and right panels are significant due to the degeneracy breaking power of the additional data in these planes. For this model, the combined constraints on $\Omega_m = 0.278^{+0.012}_{-0.011}$ and $H_0 = 70.0 \pm 1.3$ km s⁻¹Mpc⁻¹ are again very tight.

6 DISCUSSION

6.1 Comparing results

For a Λ CDM expansion model, and combining galaxy and CMB data, recent studies have presented constraints on γ

which is highly correlated with $\Omega_c h^2$ ($\rho = 0.92$) and is purely an expansion parameter at high- z (see the definition and further details in e.g. Komatsu et al. 2009), is also large, $\rho = 0.68$. The correlations between γ and $\Omega_m (= \Omega_b + \Omega_c)$, $\rho = 0.32$, γ and $\Omega_b h^2$, $\rho = 0.11$, and γ and H_0 , $\rho = 0.13$, are significantly smaller. As shown in the right panel of Figure 3 for other data combinations, the correlation between Ω_m and H_0 is also large, $\rho = -0.82$.

²⁷ <http://www.esa.int/Planck>

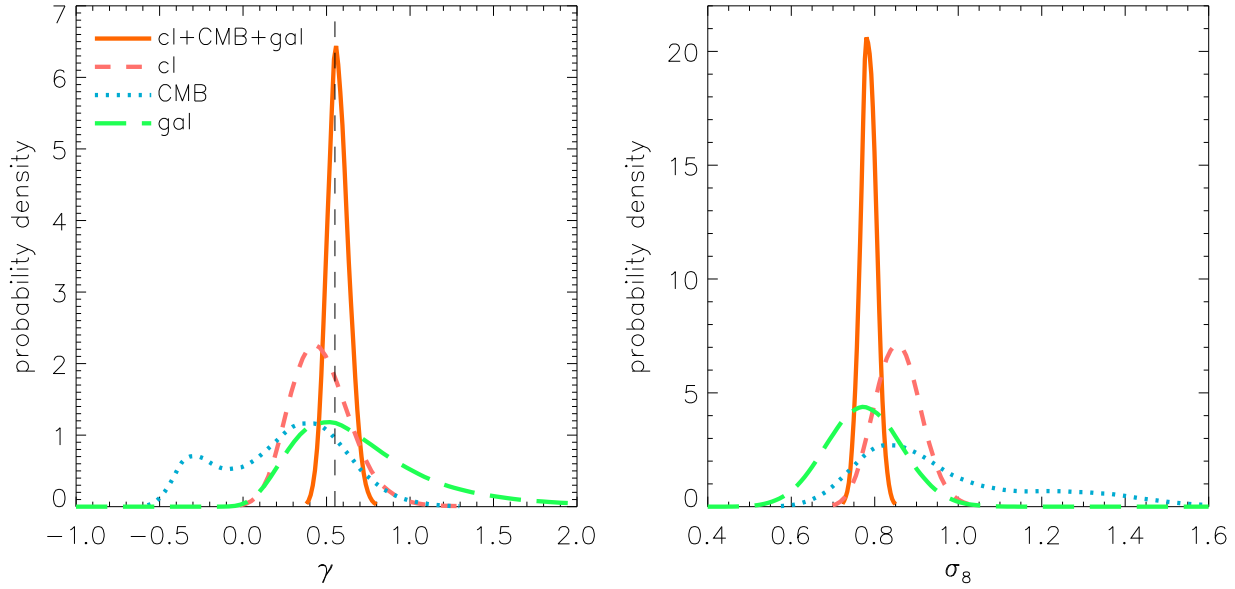


Figure 4. Marginalized probability distribution functions for γ (left panel) and σ_8 (right panel) for the $\gamma+\Lambda$ CDM model. Results are shown for the following data sets: CMB (blue, dotted line), gal (green, long-dashed line), cl (red, dashed line) and cl+CMB+gal (gold, solid line). In the left panel, the vertical, dashed line marks $\gamma = 0.55$ (GR).

that are similar to and in agreement with ours. For example, Hudson & Turnbull (2012) combined data from two peculiar velocity surveys at low redshifts (Davis et al. 2011; Turnbull et al. 2012) and RSD (but not AP effect) data from various galaxy surveys. Samushia et al. (2013) used primarily RSD, AP effect, and BAO data from the CMASS BOSS results of Reid et al. (2012) together with RSD and AP effect data from other surveys. In their combined results, both studies include WiggleZ, 6dFGS and CMASS BOSS data, as we do here, in addition to other galaxy and expansion data sets. Both analyses use CMB data from *WMAP7*. The former study uses previous results from CMB and expansion data only as a prior, while the latter uses the full CMB likelihood²⁸. Neither of these analyses, however, use the low multipoles of the CMB to constrain γ with the ISW effect (see Section 6.1.1).

Note also that these studies include BAO constraints from Percival et al. (2010) and Reid et al. (2012), respectively. As discussed in Section 6.1.2, both BAO data sets (and especially the latter) prefer larger values for Ω_m , which in combination with growth data implies a preference for larger values of γ . This, together with the fact that these works do not include the cluster data or the ISW effect constraints from the CMB data, which both prefer smaller values for γ , is consistent with their results on γ being at the high end of ours in Table 1. Although all these results and those in Table 1 are consistent with GR ($\gamma \simeq 0.55$), the differences highlight the importance of studying each

individual data set as well as their various combinations in detail before combining all of them. For upcoming, more statistically powerful data sets, this will also be increasingly important.

6.1.1 ISW effect

Even though the ISW effect has only a relatively small impact on the combined results, it is not negligible. Using our analysis, it is interesting to compare results including or not the ISW effect for γ . For the $\gamma+\Lambda$ CDM model and the combination CMB+gal, we obtain $\gamma = 0.607^{+0.078}_{-0.080}$ without the ISW effect, which as expected (see Section 6.2) is slightly higher (3 per cent) than our default result (see Table 1) and weaker by 8 per cent.²⁹ For cl+CMB, we obtain $\gamma = 0.432^{+0.152}_{-0.153}$ and $\sigma_8 = 0.842 \pm 0.057$, which are 20 and 16 per cent weaker than our default results (see also a similar comparison in Rapetti et al. 2009). For cl+CMB+gal, $\gamma = 0.585 \pm 0.067$ is only 6 per cent weaker than the corresponding result including the ISW effect for γ .

6.1.2 Adding the BAO data

Our results show (see both Table 1 and the left panel of Figure 4) that, compared with the cluster and CMB data, the

²⁸ Note that it is important to include γ in the full CMB analysis, in combination with the other experiments, to account for all the degeneracies of the CMB parameters with both expansion and growth parameters, such as e.g. that of γ with $\Omega_c h^2$ or the CMB shift parameter. If these covariances are not included, one may obtain spuriously tight results.

²⁹ For the same data but for the $\gamma+w$ CDM model, we obtain $\gamma = 0.547^{+0.092}_{-0.093}$, higher by 4 per cent and weaker by 5 per cent, and $w = -0.914 \pm 0.073$, tighter by 10 per cent. For this model, the background expansion parameter w modifies the ISW effect in an approximately opposite way to that of the density perturbation parameter γ . Therefore, by artificially ignoring γ in the calculation of the ISW effect, tighter constraints on w are obtained. This is comparable to what happens for a w -model of a dark energy fluid when its dark energy perturbations are erroneously not taken into account (Weller & Lewis 2003; Bean & Dore 2004; Rapetti et al. 2005).

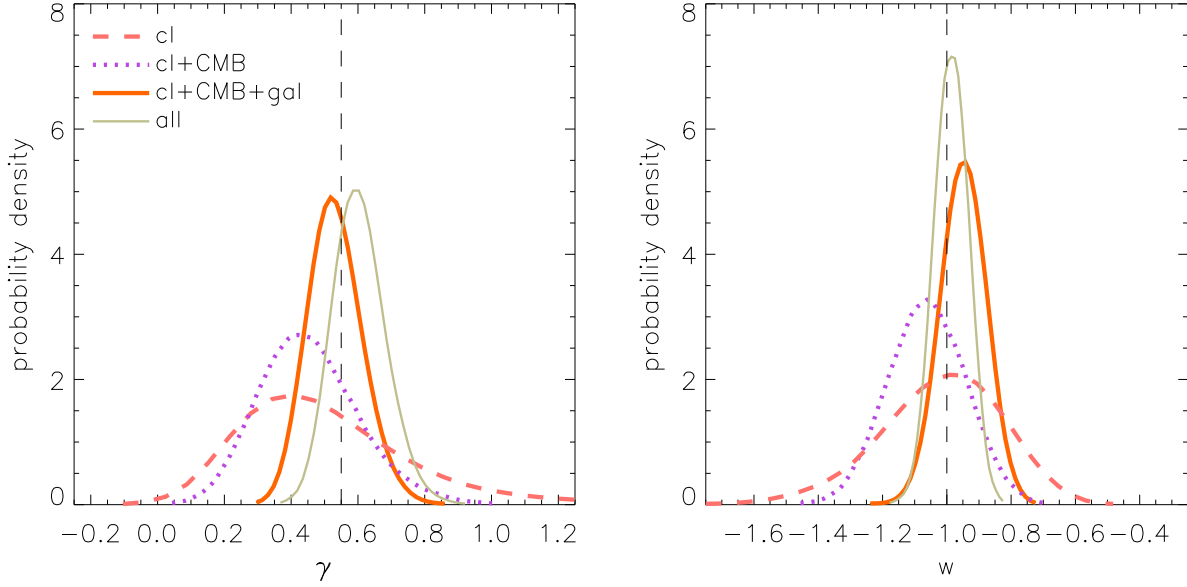


Figure 5. Marginalized probability distribution functions for γ (left panel) and w (right panel) for the $\gamma+w$ CDM model. Results are shown for the following data sets: cl (red, dashed line), cl+CMB (purple, dotted line), cl+CMB+gal (gold, solid line) and cl+CMB+gal+SNIa+SH0ES+BAO (platinum, solid-thin line). The vertical, dashed lines mark $\gamma = 0.55$ (GR; left panel) and $w = -1$ (Λ CDM; right panel). Note that γ (cosmic growth) and w (cosmic expansion) are measured simultaneously with similar precision.

combination gal+BAO prefers significantly larger values of Ω_m , and therefore of γ due to the covariances between Ω_m and γ , and Ω_m and σ_8 (see Section 5.1).³⁰ Also, for any of the data set combinations in Table 1, the addition of the BAO data shifts the constraints on Ω_m and γ to larger values. Adding BAO to all the other data sets combined and for the $\gamma+w$ CDM model, we have increases of 9 and 12 per cent for each parameter³¹. It is interesting to note, though, that using only the BOSS BAO data set, we obtain similar shifts of 7 and 11 per cent, although slightly weaker constraints on Ω_m , and similar constraints on γ . Using instead only the BAO data set of Percival et al. (2010), we find about half of those increases, 5 per cent for both parameters, and also a bit weaker constraints on Ω_m . The constraints on γ , though, are slightly tighter due to the reduction in the tension with the other data sets. The mild tension on Ω_m between the BAO and the other data sets translates in some cases into a smaller constraining power for γ (and also for w) when combining them. Table 1 shows e.g. that for $\gamma+w$ CDM, adding both BAO data sets to cl+CMB+gal provides somewhat weaker constraints on γ , and also that these are 13 per cent weaker than those for instead adding SNIa to cl+CMB+gal. In addition, using all the data sets combined except BAO, we obtain the tightest constraints on γ for $\gamma+\Lambda$ CDM, and on both γ and w for $\gamma+w$ CDM. However, the increase in constraining power on these parameters is small compared

with the decrease in constraining power on the other expansion parameters when not using BAO.

The BAO and SH0ES data also present a mild tension in the direction of the well-known degeneracy between H_0 and Ω_m (see e.g. Hinshaw et al. 2012). The addition of SH0ES to any of the data combinations in Table 1 that include our primary data sets, shifts H_0 to larger values, and therefore Ω_m to smaller values through the correlation between these two parameters.

6.2 Constraining power

As discussed in Section 5.2, the combination CMB+gal provides tight constraints on the σ_8, γ plane (see Figure 1) due to the complementarity between the constraints from the individual data sets. However, the large degeneracies of the individual constraints make the combination prone to potential biases from systematic uncertainties. The left panel of Figure 4 shows that for galaxies alone (green, long-dashed line) the marginalized pdf for γ has a large tail toward values higher than that for GR, although interestingly the peak is close to the GR value (vertical, dashed line).³² On the other hand, for the CMB (blue, dotted line) values larger than that for GR are significantly constrained by the data (due to the ISW effect), while lower values are largely unconstrained and degenerate with σ_8 , which has an extended tail toward large values (see the right panel of the figure).

From comparing the normalized pdf's in the figure, it is worth noting that while the constraining power of the cluster data on γ (left panel) and σ_8 (right panel) is notably

³⁰ For $\gamma+\Lambda$ CDM, using the CMB data alone we have $\Omega_m = 0.260 \pm 0.030$. For gal+BAO, using only the BAO data set from Percival et al. (2010), we obtain $\Omega_m = 0.345 \pm 0.050$ and $\gamma = 0.719^{+0.244}_{-0.245}$, and using instead only the BOSS BAO data set, $\Omega_m = 0.417 \pm 0.073$ and $\gamma = 0.978^{+0.350}_{-0.363}$, which are clearly larger.

³¹ Note that the shift between the gold, solid and platinum, solid-thin lines in Figure 5 is mainly due to the addition of BAO.

³² Adding the expansion data set BAO to gal shortens this tail (see Figure 1) and shifts the peak to a larger value (see Table 1).

better than that of the CMB or galaxy data, the combination cl+CMB+gal is much more powerful than the cluster data alone. Note also that the power of the current data for constraining σ_8 (right panel) is considerably greater than for constraining γ (left panel).

6.2.1 Full model: $\gamma+w\Lambda\text{CDM}$

For our most general model, $\gamma+w\Lambda\text{CDM}$, only the cluster data can alone constrain this model at a significant level. We obtain $w = -1.021^{+0.190}_{-0.187}$ and $\gamma = 0.507^{+0.236}_{-0.242}$ (see also Figure 5).³³ Since our other primary data sets do not have strong direct constraints on γ (see Section 3), their constraining power depends critically on the complexity of the model used. For our extended model, we allow departures from the standard expansion and growth histories equally. Combining all our data sets, we obtain the tightest and most robust results to date on this model. The addition of SNIa, SH0ES and BAO data is particularly helpful for constraining the expansion parameters in this model. The right panel of Figure 5 shows that when we include these data sets (platinum, solid-thin line) the constraining power on w clearly increases. The figure also shows the progression in the pdf's of γ (left panel) and w (right panel) when adding one at a time the other primary data sets to the cluster data. Remarkably, for these combinations (as well as for the others of the primary data sets) we can measure at the same time γ (cosmic growth) and w (cosmic expansion) with similar precision.

7 CONCLUSIONS

We have combined cluster growth and f_{gas} data from RASS and CXO, CMB data from *WMAP*, and RSD and AP effect data from WiggleZ, 6dFGS and CMASS BOSS to simultaneously constrain the evolution of cosmic structure and background expansion. To test for consistency with GR and ΛCDM , we have used convenient parameterizations: Ω_m , H_0 and w for the expansion history, and σ_8 and γ for the growth history. We find that the combination of clusters+CMB+galaxies breaks key degeneracies in the growth plane, σ_8 versus γ , for the data sets individually. In combination, the data provide tight, robust constraints that are in excellent agreement with GR+ ΛCDM .

Fixing $w = -1$, we obtain marginalized constraints on the growth parameters $\sigma_8 = 0.785 \pm 0.019$ and $\gamma = 0.570^{+0.064}_{-0.063}$. Including SNIa, SH0ES and BAO data we obtain $\gamma = 0.616 \pm 0.061$. Allowing w to vary, we have $\sigma_8 = 0.780 \pm 0.020$ and $\gamma = 0.533 \pm 0.080$ for the combination of clusters+CMB+galaxies. For this, we find a correlation between w and γ of $\rho = -0.66$. Including SNIa+SH0ES+BAO, we obtain $\Omega_m = 0.278^{+0.012}_{-0.011}$, $H_0 = 70.0 \pm 1.3 \text{ km s}^{-1} \text{ Mpc}^{-1}$ and $w = -0.987^{+0.054}_{-0.053}$ for the expansion parameters, and $\sigma_8 = 0.789 \pm 0.019$ and $\gamma = 0.604 \pm 0.078$ for the growth parameters.

³³ For the combination gal+BAO (see Table 1), we obtain similar constraints on w and γ , while those on Ω_m and σ_8 are notably weaker.

Our results highlight the potential of combining forthcoming galaxy cluster data (from e.g. the South Pole Telescope [SPT], the Atacama Cosmology Telescope [ACT], XMM-*Newton* wide area surveys, the Dark Energy Survey [DES], the Large Synoptic Survey Telescope [LSST], and the extended *ROentgen* Survey with an Imaging Telescope Array [eROSITA]), CMB data (from e.g. SPT, ACT and *Planck*), and galaxy data (from e.g. SDSS-III, the Subaru Measurement of Images and Redshifts [SuMIRe] project, BigBOSS, the Dark Energy Spectrometer [DESpec], and the Euclid mission) for constraining dark energy and modified gravity models.

ACKNOWLEDGMENTS

We thank the anonymous referee for useful comments and G. Morris for technical support. The computational analysis was carried out using the KIPAC XOC, orange and pinto clusters at SLAC. The Dark Cosmology Centre (DARK) is funded by the Danish National Research Foundation. DR acknowledges support from the DARK Fellowship program. CB acknowledges the support of the Australian Research Council through the award of a Future Fellowship. AM acknowledges support from grant NSF AST-0838187. FB acknowledges support from the Australian Government through the International Postgraduate Research Scholarship (IPRS). We acknowledge support from the National Aeronautics and Space Administration (NASA) through *Chandra* Award Number TM1-12010X issued by the *Chandra* X-ray Observatory Center, which is operated by the Smithsonian Astrophysical Observatory for and on behalf of NASA under contract NAS8-03060. This work was supported in part by the U.S. Department of Energy under contract number DE-AC02-76SF00515. We also thank DARK and the Niels Bohr International Academy for hospitality during the 2011 Summer workshop in which this work was initiated.

REFERENCES

- Abazajian K. N. et al., 2009, *ApJS*, 182, 543
- Acquaviva V., Hajian A., Spergel D. N., Das S., 2008, *Phys. Rev. D*, 78, 043514
- Allen S. W., Evrard A. E., Mantz A. B., 2011, *Ann. Rev. Astr. Astrophys.*, 49, 409
- Allen S. W., Rapetti D. A., Schmidt R. W., Ebeling H., Morris R. G., Fabian A. C., 2008, *MNRAS*, 383, 879
- Amin M. A., Wagoner R. V., Blandford R. D., 2008, *MNRAS*, 390, 131
- Anderson L. et al., 2012, *MNRAS*, 427, 3435
- Arkani-Hamed N., Cheng H. S., Luty M. A., Mukohyama S., 2004, *J. High Energy Phys.*, 5, 74
- Ballinger W. E., Peacock J. A., Heavens A. F., 1996, *MNRAS*, 282, 877
- Basilakos S., Pouri A., 2012, *MNRAS*, 423, 3761
- Bean R., Dore O., 2004, *Phys. Rev. D*, 69, 083503
- Bennett C. L. et al., 2012, preprint (arXiv:1212.5225)
- Bertschinger E., Zukin P., 2008, *Phys. Rev. D*, 78, 024015
- Beutler F. et al., 2012, *MNRAS*, 423, 3430
- Blake C. et al., 2011a, *MNRAS*, 415, 2876

- Blake C. et al., 2011b, MNRAS, 418, 1707
 Blake C. et al., 2011c, MNRAS, 418, 1725 (B11)
 Blake C. et al., 2012, MNRAS, 425, 405
 Bryan G. L., Norman M. L., 1998, ApJ, 495, 80
 Carroll S. M., Duvvuri V., Trodden M., Turner M. S., 2004, Phys. Rev. D, 70, 043528
 Challinor A., Lasenby A., 1999, ApJ, 513, 1
 Clifton T., Ferreira P. G., Padilla A., Skordis C., 2012, Phys. Rep., 513, 1
 Colless M. et al., 2003, preprint (arXiv:0306581)
 Conley A. et al., 2011, ApJS, 192, 1
 Copeland E. J., Sami M., Tsujikawa S., 2006, Int. J. Modern Phys. D, 15, 1753
 Daniel S. F., Linder E. V., Smith T. L., Caldwell R. R., Cooray A., Leauthaud A., Lombriser L., 2010, Phys. Rev. D, 81, 123508
 Davis M., Nusser A., Masters K. L., Springob C., Huchra J. P., Lemson G., 2011, MNRAS, 413, 2906
 de Rham C., Gabadadze G., Tolley A. J., 2011, Phys. Rev. Lett., 106, 231101
 Di Porto C., Amendola L., 2008, Phys. Rev. D, 77, 083508
 Drinkwater M. J. et al., 2010, MNRAS, 401, 1429
 Dunkley J. et al., 2009, ApJS, 180, 306
 Dvali G., Gabadadze G., Porrati M., 2000, Phys. Lett. B, 485, 208
 Eisenstein D. J., Hu W., 1998, ApJ, 496, 605
 Eisenstein D. J. et al., 2011, AJ, 142, 72
 Frieman J. A., Turner M. S., Huterer D., 2008, ARA&A, 46, 385
 Giannantonio T., Martinelli M., Silvestri A., Melchiorri A., 2010, J. Cosmol. Astropart. Phys., 4, 30
 Gong Y., Ishak M., Wang A., 2009, Phys. Rev. D, 80, 023002
 Hamann J., Hannestad S., Lesgourgues J., Rampf C., Wong Y. Y. Y., 2010, J. Cosmol. Astropart. Phys., 7, 22
 Hamann J., Hannestad S., Raffelt G. G., Wong Y. Y. Y., 2007, J. Cosmol. Astropart. Phys., 8, 21
 Hinshaw G. et al., 2012, preprint (arXiv:1212.5226)
 Hojjati A., Pogosian L., Zhao G.-B., 2011, J. Cosmol. Astropart. Phys., 8, 5
 Hu W., Sawicki I., 2007, Phys. Rev. D, 76, 104043
 Hudson M. J., Turnbull S. J., 2012, ApJ, 751, L30
 Jarrett T. H., Chester T., Cutri R., Schneider S., Skrutskie M., Huchra J. P., 2000, AJ, 119, 2498
 Jennings E., Baugh C. M., Pascoli S., 2011, MNRAS, 410, 2081
 Jones D. H. et al., 2009, MNRAS, 399, 683
 Kaiser N., 1986, MNRAS, 222, 323
 Komatsu E. et al., 2009, ApJS, 180, 330
 Komatsu E. et al., 2011, ApJS, 192, 18
 Kosowsky A., Milosavljevic M., Jimenez R., 2002, Phys. Rev. D, 66, 063007
 Lewis A., Bridle S., 2002, Phys. Rev. D, 66, 103511
 Lewis A., Challinor A., Lasenby A., 2000, ApJ, 538, 473
 Linder E. V., 2005, Phys. Rev. D, 72, 043529
 Linder E. V., Cahn R. N., 2007, Astropart. Phys., 28, 481
 Lombriser L., Schmidt F., Baldauf T., Mandelbaum R., Seljak U., Smith R. E., 2012, Phys. Rev. D, 85, 102001
 Mantz A., Allen S. W., Ebeling H., Rapetti D., 2008, MNRAS, 387, 1179
 Mantz A., Allen S. W., Rapetti D., Ebeling H., 2010a, MNRAS, 406, 1759 (M10a)
 Mantz A., Allen S. W., Ebeling H., Rapetti D., Drlica-Wagner A., 2010b, MNRAS, 406, 1773 (M10b)
 Masters K. L. et al., 2011, MNRAS, 418, 1055
 Matsubara T., 2000, ApJ, 535, 1
 Matsubara T., Suto Y., 1996, ApJ, 470, L1
 Nesseris S., Perivolaropoulos L., 2008, Phys. Rev. D, 77, 023504
 Nicolis A., Rattazzi R., Trincherini E., 2009, Phys. Rev. D, 79, 064036
 Peebles P. J. E., 1980, The large-scale structure of the universe. Princeton University Press, Princeton, NJ
 Percival W. J. et al., 2010, MNRAS, 401, 2148
 Perlmutter S. et al., 1999, ApJ, 517, 565
 Pettini M., Zych B. J., Murphy M. T., Lewis A., Steidel C. C., 2008, MNRAS, 391, 1499
 Polarski D., Gannouji R., 2008, Phys. Lett., B660, 439
 Rapetti D., Allen S. W., Mantz A., Ebeling H., 2009, MNRAS, 400, 699
 Rapetti D., Allen S. W., Mantz A., Ebeling H., 2010, MNRAS, 406, 1796 (R10)
 Rapetti D., Allen S. W., Weller J., 2005, MNRAS, 360, 555
 Reid B. A. et al., 2012, MNRAS, 426, 2719
 Reid B. A., White M., 2011, MNRAS, 417, 1913
 Reyes R., Mandelbaum R., Seljak U., Baldauf T., Gunn J. E., Lombriser L., Smith R. E., 2010, Nat, 464, 256
 Riess A. G. et al., 1998, AJ, 116, 1009
 Riess A. G. et al., 2011, ApJ, 730, 119
 Samushia L. et al., 2013, MNRAS, 429, 1514
 Schmidt F., Vikhlinin A., Hu W., 2009, Phys. Rev. D, 80, 083505
 Seo H.-J., Eisenstein D. J., 2003, ApJ, 598, 720
 Simpson F. et al., 2013, MNRAS, 429, 2249
 Simpson F., Peacock J. A., 2010, Phys. Rev. D, 81, 043512
 Song Y.-S., Percival W. J., 2009, J. Cosmol. Astropart. Phys., 10, 4
 Spergel D. N. et al., 2007, ApJS, 170, 377
 Spergel D. N. et al., 2003, ApJS, 148, 175
 Suzuki N. et al., 2012, ApJ, 746, 85
 Tinker J., Kravtsov A. V., Klypin A., Abazajian K., Warren M., Yepes G., Gottlöber S., Holz D. E., 2008, ApJ, 688, 709
 Turnbull S. J., Hudson M. J., Feldman H. A., Hicken M., Kirshner R. P., Watkins R., 2012, MNRAS, 420, 447
 Vikhlinin A. et al., 2009, ApJ, 692, 1060
 Wang L.-M., Steinhardt P. J., 1998, ApJ, 508, 483
 Weinberg D. H., Mortonson M. J., Eisenstein D. J., Hirata C., Riess A. G., Rozo E., 2012, preprint (arXiv:1201.2434)
 Weller J., Lewis A. M., 2003, MNRAS, 346, 987
 Wojtak R., Hansen S. H., Hjorth J., 2011, Nat, 477, 567
 Zhang P., Liguori M., Bean R., Dodelson S., 2007, Phys. Rev. Lett., 99, 141302
 Zhao G.-B., Giannantonio T., Pogosian L., Silvestri A., Bacon D. J., Koyama K., Nichol R. C., Song Y.-S., 2010, Phys. Rev. D, 81, 103510
 Zhao G.-B., Li H., Linder E. V., Koyama K., Bacon D. J., Zhang X., 2012, Phys. Rev. D, 85, 123546